

Molecular Engineering of Thiazole Orange Dye: Change of Fluorescent Signaling from Universal to Specific upon Binding with Nucleic Acids in Bioassay

Yu-Jing Lu,^{*,†} Qiang Deng,[†] Jin-Qiang Hou,[§] Dong-Ping Hu,[†] Zheng-Ya Wang,[†] Kun Zhang,[†] Leonard G. Luyt,^{§,||} Wing-Leung Wong,^{*,‡} and Cheuk-Fai Chow[‡]

[†]Institute of Natural Medicine and Green Chemistry, School of Chemical Engineering and Light Industry, Guangdong University of Technology, Guangzhou 510006, Peoples' Republic of China

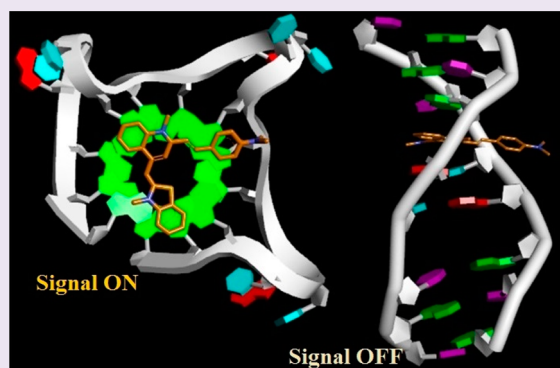
[‡]Department of Science and Environmental Studies, Centre for Education in Environmental Sustainability, The Hong Kong Institute of Education, 10 Lo Ping Road, Tai Po, Hong Kong SAR, Peoples' Republic of China

[§]London Regional Cancer Program, 790 Commissioners Road East, London, Ontario N6A 4L6, Canada

^{||}Departments of Oncology, Chemistry, Medical Imaging, The University of Western Ontario, London, Ontario N6A 3K7, Canada

Supporting Information

ABSTRACT: The universal fluorescent staining property of thiazole orange (TO) dye was adapted in order to be specific for G-quadruplex DNA structures, through the introduction of a styrene-like substituent at the ortho-position of the TO scaffold. This extraordinary outcome was determined from experimental studies and further explored through molecular docking studies. The molecular docking studies help understand how such a small substituent leads to remarkable fluorescent signal discrimination between G-quadruplex DNA and other types of nucleic acids. The results reveal that the modified dyes bind to the G-quadruplex or duplex DNA in a similar fashion as TO, but exhibit either enhanced or quenched fluorescent signal, which is determined by the spatial length and orientation of the substituent and has never been known. The new fluorescent dye modified with a p-(dimethylamino)styryl substituent offers 10-fold more selectivity toward telomeric G-quadruplexes than double-stranded DNA substrates. In addition, native PAGE experiments, FRET, CD analysis, and live cell imaging were also studied and demonstrated the potential applications of this class of thiazole-orange-based fluorescent probes in bioassays and cell imaging.



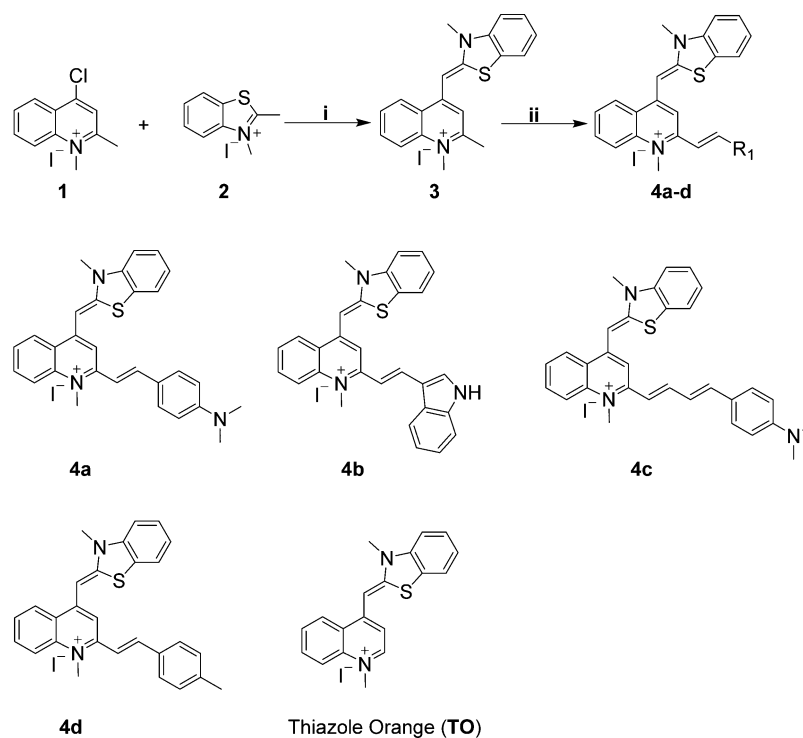
The development of highly sensitive and selective probes to qualitatively and quantitatively detect nucleic acids is extremely important for a wide range of investigations,^{1–4} such as the active research areas of chemical biology, biochemistry, and clinical diagnosis. The prototypical nucleic acid DNA, apart from forming primarily double helical structures, is able to adopt higher-ordered and functionally useful structures. G-quadruplex is one such distinctive structure, which forms a unique four-stranded structure containing guanine-rich nucleic acids sequences.^{5,6} G-quadruplexes can be divided into three primary topologies: parallel, antiparallel, and hybrid-type structures.⁷ These unique sequences can be found in some important genomic regions, such as telomere, rDNA, promoter regions of some oncogenes, and the untranslated regions of mRNA.^{8–10} In recent years, G-quadruplex structures have received attention because their unique structural features are believed to be able to provide biological significance in telomere maintenance, transcription regulation, and antitumor chemotherapy.^{11–18} G-quadruplex binders have great potential for development as anticancer drugs with the expected outcome

for research in this area being eventual translation to the clinic. Since G-rich telomeric DNA sequences synthesized by telomerase have been shown to form G-quadruplexes *in vivo*,^{11,15,16} telomeric G-quadruplexes therefore attract tremendous interest and research effort.^{12,18} Moreover, G-quadruplexes were demonstrated as versatile building blocks that offer substantial advantages on fluorescence sensors.^{19,20}

Small molecule based fluorescent probes have been identified for *in vitro* or *in vivo* analysis of G-quadruplex DNA,²¹ such as triphenylmethane dyes,²² cyanovinyl-pyridinium triphenylamine,²³ and triarylimidazole (IZCM-1).²⁴ Among the reported studies, thiazole orange (TO) is one of the most widely used fluorescent probes in nucleic acid staining due to its high fluorescence quantum yield.^{25–27} However, TO is a universal nucleic acid fluorescent dye which has no ability to differentiate

Received: November 30, 2015

Accepted: January 11, 2016

Scheme 1. Synthesis Route to 4a–4d and Their Molecular Structures^a

^aReagents and conditions: (i) NaHCO₃, methanol, room temp., 1 h; (ii) reaction with aromatic aldehydes, 135 °C, reflux 3 h.

G-quadruplex DNA from other DNA species. A recent approach is to develop a new generation of G-quadruplex selective fluorescent probes by the integration of a G-quadruplex selective binder into a TO molecule. Successful examples include benzofuroquinolinium,^{28,29} ISTO,³⁰ TOPI,³¹ PyroTASQ,³² and PDC-TO,³³ demonstrating that the structural modification on the basis of the TO framework is able to provide direct and remarkable G-quadruplex specificity and/or fluorescence discrimination. Recently, a styryl-substituted TO molecule was developed as a RNA fluorescent dye.³⁴ Currently, how a small substituent such as a styryl group allied to a TO molecule can induce signaling specificity is unclear and has not been discussed in the literature. We believe that understanding the fundamentals on the relationship of interaction and signaling between the dye and DNA at the molecular level is very important for structure-based probe design either for biosensing or for drug target applications. In the present study, we report on a series of new fluorescent dyes, designed on the basis of a TO framework by systematically introducing various styrene-like substituents at its ortho-position, and investigate the influence on the binding property and fluorescence discrimination with various duplex and G-quadruplex-DNA substrates through both experimental and modeling studies. These TO derived dyes are able to bind with nucleic acids, and surprisingly, excellent fluorescent signal discrimination is found to be determined by the spatial length and orientation of a small substituent of the TO molecule. In addition, the photophysical properties of the dyes, including fluorescence quantum yields, equilibrium binding constants, the detection limit toward G-quadruplex-DNA, and their potential applications in live cell staining and imaging, were explored.

2. RESULTS AND DISCUSSION

2.1. Synthesis of New Fluorescent Dyes. Intermediate 1 (4-chloro-1,2-dimethylquinolin-1-ium iodide) was obtained by the reaction of 4-chloro-2-methylquinoline with iodomethane. This was followed by reaction with 2,3-dimethylbenzo[d]thiazol-3-ium iodide (2) to give compound 3 ((Z)-1,2-dimethyl-4-((3-methylbenzo[d]thiazol-2(3H)-ylidene)methyl)quinolin-1-ium iodide) as the key intermediate.³⁵ A series of the targeted thiazole orange based fluorescent dyes 4a–4d (Scheme 1) with different styryl substituents introduced at its ortho-position was synthesized by the reaction of 3 with a variety of aromatic aldehydes including p-dimethylaminobenzaldehyde (4a), indole-2-carboxaldehyde (4b), p-(dimethylamino)cinnamaldehyde (4c), and p-methylbenzaldehyde (4d). The compounds were obtained with high isolated yields (83–90%). The purity of the compounds was confirmed to be above 95% by using HPLC analysis.

2.2. Fluorescence Discrimination of the Dyes toward Different DNA Substrates and the Comparison of Their Binding Kinetics. As indicated from the screening results shown in Figure 1, the parent TO dye provides no selectivity, and fluorescence is increased by both dsDNA and G4-DNA, while the four styryl modified dyes show impressive fluorescent signal discrimination that is specific to G-quadruplex DNA. For the modified TO compounds, both ssDNA and dsDNA substrates give very weak fluorescent signal induction. The binding behavior and specificity of 4a–4d toward a number of nucleic acids were evaluated. The experiments were conducted using fluorescence titration with 20 targeted nucleic acids including single-stranded DNA (ssDNA), double-stranded DNA (dsDNA), G-quadruplex DNA (G4-DNA), and RNA.³⁴ Generally, as shown in Figure 1, the fluorescence intensity of the TO dyes after modification with a styryl substituent are

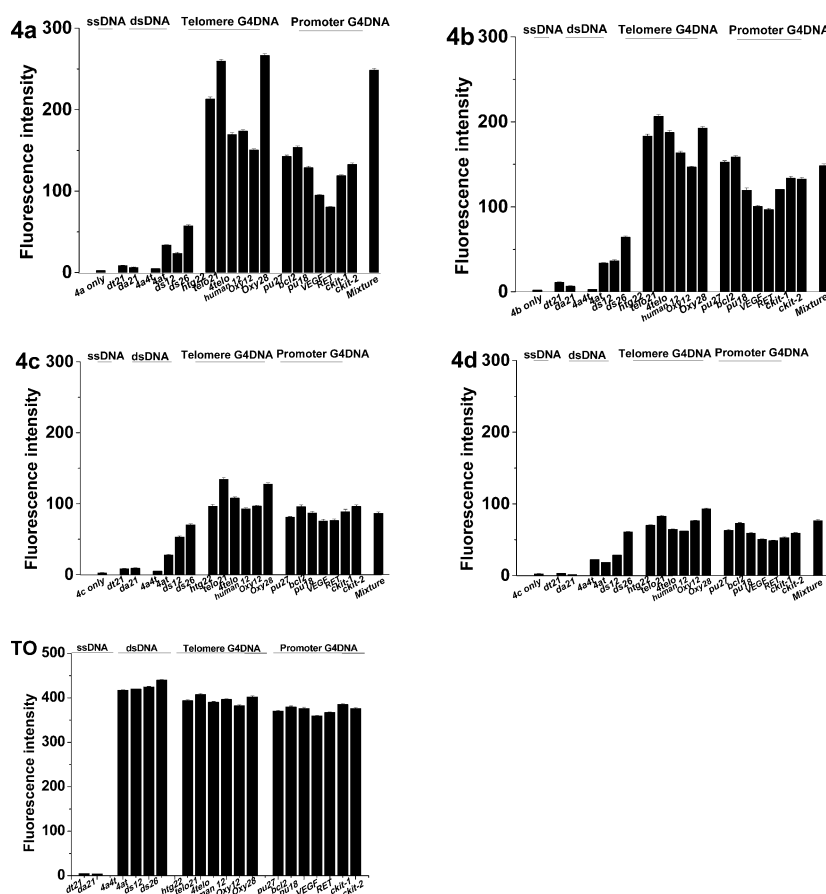


Figure 1. Fluorescence intensities at 630 nm ($\lambda_{\text{ex}} = 475$ nm) of **4a–4d** and **TO** with different nucleic acids in Tris–HCl buffer containing 60 mM KCl. Single-stranded DNA: da21, dt21. Duplex DNA: 4a4t, 4at, ds12, and ds26. Telomere G-quadruplex DNA: htg22, telo21, 4telo, human 12, oxy12, and oxy28. Promoter G-quadruplex DNA: bcl2, ckit-1, ckit-2, Pu27, Pu18, RET, and VEGF. Concentration of dye was 5 μM , and DNA concentration was 10 μM . The mixture solutions were 10 μM dt21, 10 μM ds26, 10 μM telo21, and 10 μM bcl2. The fluorescence intensity is the average of three repeated tests.

preferentially retained with G-quadruplexes' DNA over dsDNA and ssDNA (Figure S6). However, their fluorescence intensities induced upon interaction were found to be quite varied. It seems that for performance of DNA substrate discrimination in terms of induced fluorescence signal changes, compound **4a** is the best, and the remaining are in the following order: **4b** > **4c** > **4d**. Both **4c** and **4d** show poor differential ability for discriminating between dsDNA and G-quadruplex DNA. From the screening tests, it is interesting that **TO** showed a very stable response for DNA substrates in the same types of DNA, while **4a** gave a fluctuation of response toward various G4-DNA substrates; for instance, the fluorescent intensities for telo 21 and oxy 28 were largest in Telomere G4-DNA and less intensive signals for promoter G4-DNA. The observation may imply that the introduced styrene-like substituents at the ortho-position of **TO** show significant influence on binding preference due to the difference of binding orientation in the G4-DNA pockets, which can be further elaborated in the modeling study.

The binding kinetics of the dyes with different concentrations of DNA substrates including single-stranded DNA (da21), duplex-stranded DNA (ds26), G-quadruplex DNA (telo21), and RNA were performed for comparison (Figure 2). The concentration of dyes was kept constant at 5 μM in a Tris–HCl buffer containing 60 mM KCl. The fluorescence signal was measured at 630 nm ($\lambda_{\text{ex}} = 475$ nm). In general, the

dyes show preference to bind with G-quadruplex DNA over single-stranded DNA, duplex DNA, and RNA. As shown in Figure 2, **4a** exhibits much better performance than its analogues **4b–4d**. We believe this is a consequence of the effect of the substituent at the 2 position of **TO**. The binding isotherm of **4a** with telo21 quadruplex (up to 8 μM) was recorded in the presence of a large excess of duplex DNA (ds26, 100 μM ; Figure 2, **4a**). It seems that the interference from ds26 is very minor; although ds26 leads to a slight increase in the fluorescence signal, the addition of G-quadruplex DNA (telo21, 6 μM) for binding with the dye results in a remarkable induction of fluorescence intensity, more than 6 fold, compared to duplex DNA ds26 at 100 μM . The finding reveals that the telo21 quadruplex is able to displace the bound ds26 very effectively and induces a much stronger fluorescent adduct complex with **4a** *in situ* (Figure S7). The *in vitro* results prove that the new **TO** dyes are able to show high G-quadruplex binding ability in the competitive biological assay conditions.

The compounds **4a–4d** were designed with different substituents at the ortho-position of the **TO** structure, including 4-(dimethylamino)styryl, 2-vinyl-indole, 4-dimethylamino-phenyl-buta-1,3-dienyl, and 4-methylstyryl, to allow for a comparative study. These modifications may result in an improved understanding of the induction of the fluorescence signal and changes in the binding specificity of these modified

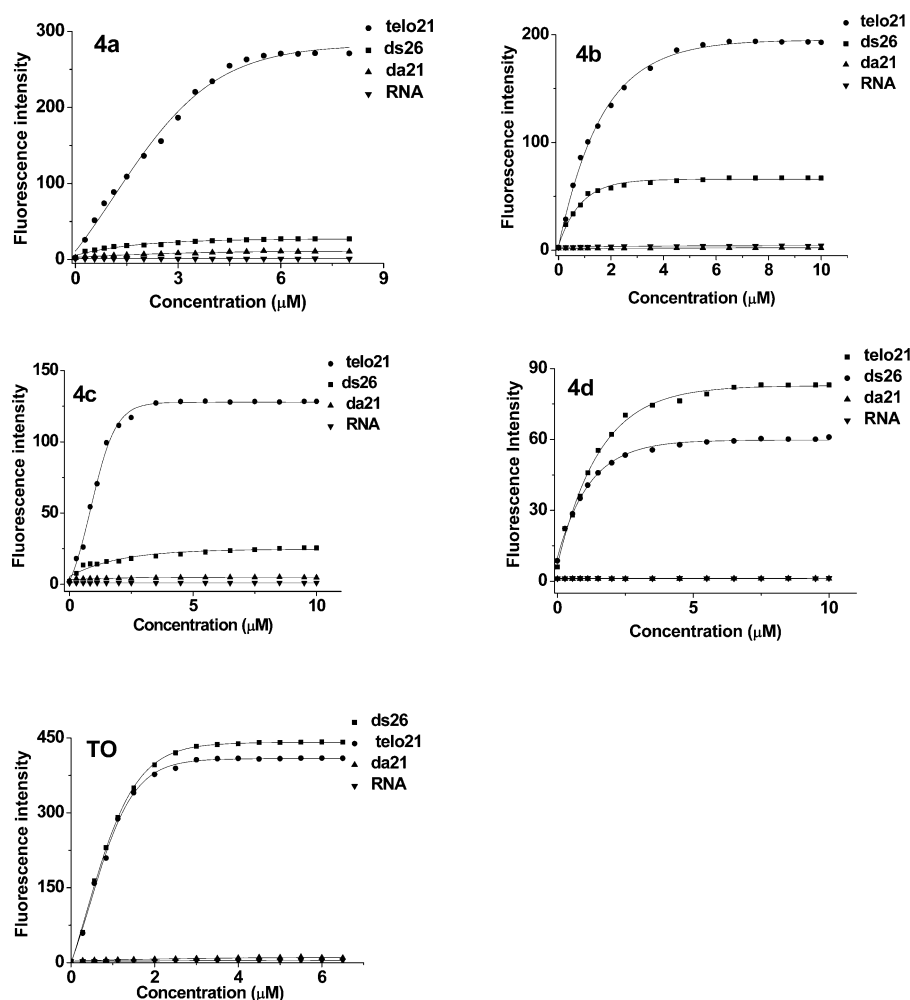


Figure 2. Binding kinetics of the dyes with different concentrations of DNA substrates: single-stranded DNAs da21, duplex-stranded DNAs ds26, G-quadruplex DNA telo21 and RNA. The concentration of dyes was 5 μM in Tris–HCl buffer containing 60 mM KCl. The fluorescence signal was measured at 630 nm ($\lambda_{\text{ex}} = 475$ nm) at 25 $^{\circ}\text{C}$.

TO dyes toward G-quadruplex DNA rather than duplex DNAs. The TO with a 4-(dimethylamino)styryl substituent (4a and 4c) demonstrated better selectivity in terms of induced fluorescence signal intensity; however, with a longer distance of the styryl substituent away from the TO structure (4c), a reduction in the induced fluorescence signal was found (Figures 1 and 2). The reasons leading to the reduction of fluorescence can be further explained by modeling studies of the substituent effects, as impacted by molecular interactions and orientation between the dye and the DNA substrate.

2.3. Spectroscopic Property, Binding Affinity, and Stabilization Studies of the Dyes with G-Quadruplex DNA. The spectroscopic properties of 4a–4d are shown in Table 1 and Table S2. The dyes structurally possess a similar conjugation scaffold, and thus the absorption maxima of the compounds in a Tris–HCl (10 mM, pH 7.4) buffer were found in the range of 465–535 nm, and the emission maxima of the dyes upon binding with telo21 were found in the range of 535–630 nm. This shift of absorption and emission maxima among the dyes is probably due to the effects of the differing substituents on the TO. Interestingly, there is an obvious trend observed in the relative fluorescence quantum yield (Φ_f), limit of detection (LOD), and equilibrium binding constant (K_d) of the dyes when interacting with telo21: 4a > 4b > 4c > 4d. This

Table 1. Spectroscopic Data of 4a–d and Their Binding Properties with telo21

ligand	absorbance (λ_{max} , nm)	E_x^a (λ_{max} , nm)	E_m (λ_{max} , nm)	Φ_f^b	LOD ^c (nM)	K_d^d ($\times 10^5 \text{ M}^{-1}$)
4a	473	475	630	0.170	2.55	9.65
4b	465	474	584	0.120	3.08	7.71
4c	474	478	535	0.103	5.86	5.38
4d	535	540	620	0.054	8.52	2.33

^aExperiments were performed in a 10 mM Tris–HCl buffer at pH 7.4. E_x is the maximum excitation wavelength; E_m is the maximum emission wavelength. ^bRelative fluorescence quantum yield of probes upon the addition of 50 μM telo21; standard of the relative fluorescence quantum yield is fluorescein ($\Phi_f = 0.85$, methanol with 1% NaOH). ^cLimit of detection for telo21. ^dEquilibrium binding constant between the compound and telo21 at 25 $^{\circ}\text{C}$.

trend may imply that the introduced substituents possibly lead to quite different interaction orientation and environment and that these could be the key sources of the resultant specificity. We believed that the K_d values are most probably depending on the binding orientation and also the extra interactions with the introduced side groups. In addition, the position of the side groups, inside or projected out of the G-quartet pocket, influences the Φ_f value. The docking study in the latter part

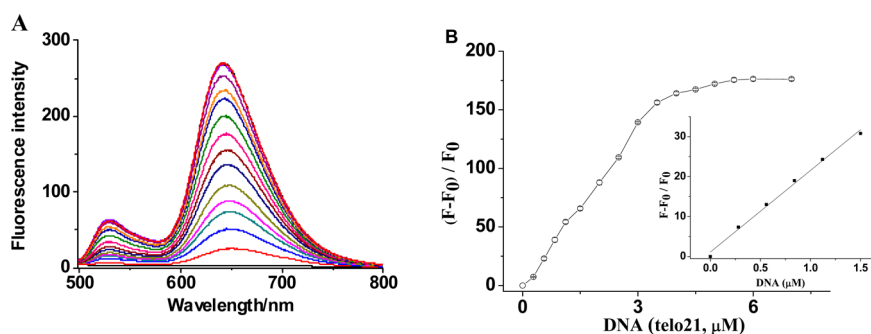


Figure 3. (A) A typical fluorescence titration spectrum of dye **4a** with telo21 in a Tris-HCl buffer (10 mM, pH 7.4). The final equivalent amount of telo21 added was 2 with respect to **4a**. (B) Fitted curve and linear relationship of **4a** with 0–1500 nM telo21. F_0 represents the fluorescence intensity without telo21, and F represents the fluorescence intensity after adding telo21.

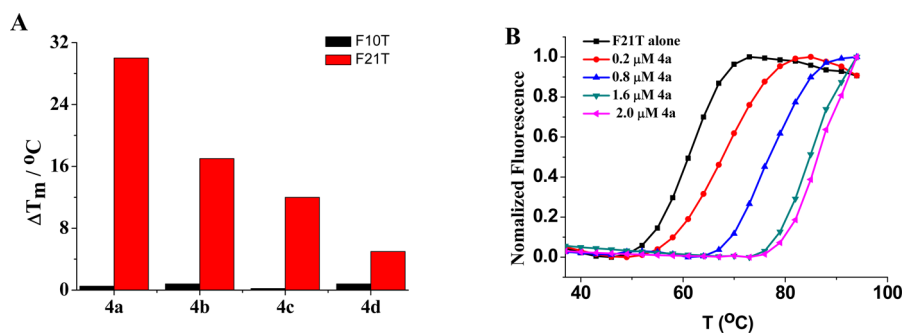


Figure 4. (A) Stabilization of G-quadruplex F21T and duplex-stranded F10T (0.4 μM) by compounds **4a–4d** (2.0 μM) in 10 mM Tris-HCl, 60 mM KCl, pH = 7.4. (B) Normalized FRET melting curves of G-quadruplex F21T (0.4 μM) at different concentrations of compound **4a** (0.2–2.0 μM) in 10 mM Tris-HCl, 60 mM KCl, pH = 7.4.

provides more information on the trends. By comparing the effects of substituents of 4-(dimethylamino)styryl (**4a**) and 4-methylstyryl (**4c**) on TO framework, **4a** shows 3 times higher fluorescence quantum yield and a K_d value with a much lower LOD value than that of **4c**. These results are also found to be in accord with the fluorescent signal enhancement (induced signal intensity: Figures 1 and 2) due to the substituent on the TO molecule. The mechanism for the fluorescent signal induction is possibly due to the suppression of free rotation of the thiazole fragment and the vibrational motions of the molecule when it is bound inside the pocket of the DNA substrate.

Human telomeric sequence telo21 (5'-GGGTTAGGGT-TAGGGTTAGGG-3') is known to form different types of G-quadruplex structures under certain incubation conditions.³⁶ For example, antiparallel G-quadruplexes are formed in Na^+ solution and hybrid-type G-quadruplexes are formed in K^+ solution. From the fluorescence titration studies with the addition of various concentrations of telo21 into **4a–4d** solutions buffered with Tris-HCl, a progressive increase in fluorescence intensity (Figure 1) was observed. The induced signal (fluorescence intensity) illustrates the effectiveness of the interaction taking place for the dyes with telo21. The results are also directly related to how significantly these substituents have effects and influence on the molecular interaction, which leads to remarkable discrimination ability toward various DNA substrates. This can be further elaborated by comparison to docking results described in the next section.

A typical fluorescence titration experiment of **4a** with G-quadruplex DNA is shown in Figure 3. The background fluorescence signal at 630 nm is very weak. A significant emission is induced upon the addition of telo21, and a plateau is reached at 6 μM . A good linear relationship for the induced

fluorescence signal and the concentration of telo21 was obtained (Figure 3B: the inserted graph, $R^2 = 0.9933$). The results suggest that the dye is a useful and selective quadruplex DNA sensor for quantitative determination and bioanalysis. The analytical parameters for limit of detection (LOD) and equilibrium binding constant (K_d) for **4a–4d** were determined and summarized in Table 1. Among the new compounds examined, LOD values vary from 2.55 nM to 8.52 nM, and **4a** exhibits the best performance with the lowest LOD (2.55 nM) and highest K_d ($9.65 \times 10^5 \text{ M}^{-1}$). Both data indicate the compound has very high G-quadruplex DNA binding specificity.

To further understand the binding properties of the dyes on the stabilization ability for the G-quadruplex structure, fluorescence resonance energy transfer (FRET) measurement was carried out, since FRET is a quantitative, rapid, and convenient method to identify promising G-quadruplex ligands and binders.^{37–39} Figure 4 shows the ΔT_m values of F21T and F10T with different concentration of **4a–4d** in a 60 mM potassium solution. The ΔT_m of F21T increased from 5 to 30 $^\circ\text{C}$ with the compounds at 2.0 μM (Figure 4A). The ΔT_m of F10T increased from 0.2 to 0.8 $^\circ\text{C}$ with the compounds at 2.0 μM (Table S4). The large ΔT_m (F21T) values compared with ΔT_m (F10T) values of the dyes are generally observed in the experiments, because the compounds are able to bind tightly with G-quadruplex DNA, and thus the G-quadruplex structure is further stabilized to give higher ΔT_m values. Among the four new ligands tested, the difference in ΔT_m (F21T) values found are very distinct and in the order of **4a** > **4b** > **4c** > **4d**. This further establishes the impact and critical role that the substituent on the TO molecule plays in the interaction with the G-quadruplex.

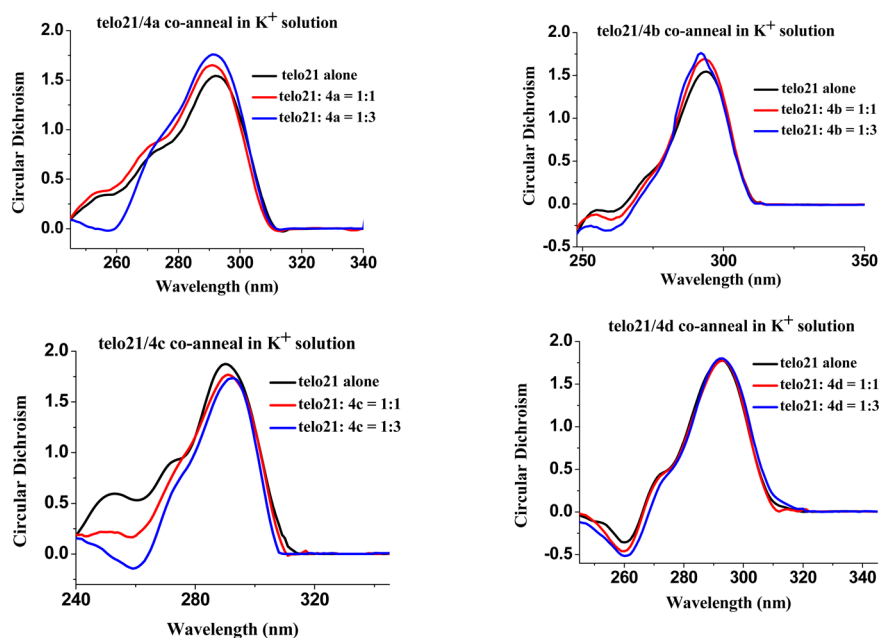


Figure 5. CD spectra of the dyes 4a–4d bound to telo21 ($5 \mu\text{M}$) in 10 mM Tris–HCl, 60 mM KCl, pH = 7.4.

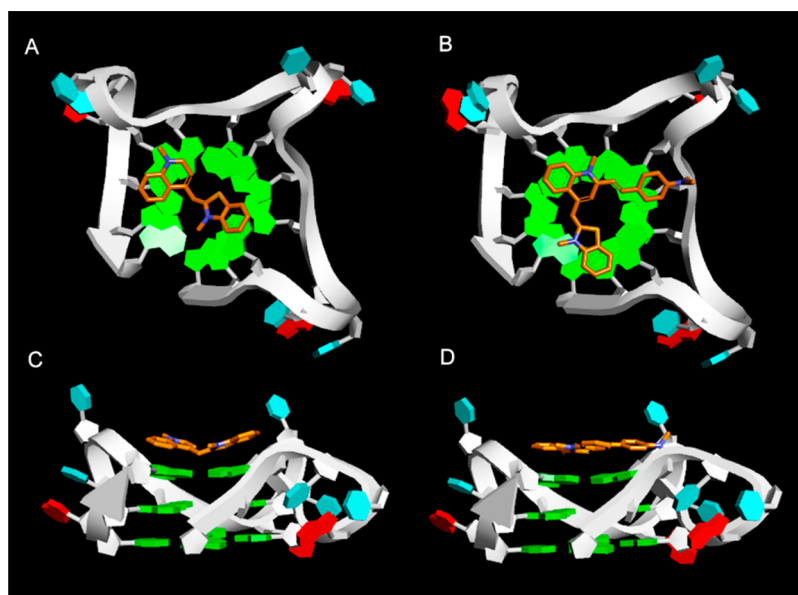


Figure 6. Top view (A, B) and side view (C, D) of the structures of Telo21 G-quadruplex in complex with TO (A, C) and 4a (B, D) from molecular docking studies.

Circular dichroism (CD) spectroscopy is a useful technique to study nucleic acid conformation and is widely used to study the G-quadruplex conversion induced by G-quadruplex binders. In the absence of TO compounds, the CD spectrum of telo21 was typical of an antiparallel G-quadruplex, with the positive peak at 290 nm and a negative peak at 265 nm.^{7,40} With the addition of 4a–4d ($15 \mu\text{M}$) to telo21 ($5 \mu\text{M}$), the characteristic peaks of the antiparallel G-quadruplex had an obvious change, with the positive peak at 290 nm gradually increasing while the negative peak at 265 nm gradually decreased as shown in Figure 5. The results indicate that the dyes have no influence on the conformation of G-quadruplexes. However, a slight enhancement of the positive peak observed may be attributed to the stabilization of G-quadruplexes by the dye. Also, the results suggest that the dyes are able to bind to G-quadruplexes, which

is consistent with the observation obtained from fluorescence titration experiments.

2.4. Modeling Study to Investigate the Influence of Styryl Substituents on the Fluorescent Discrimination Ability for G-Quadruplex DNA. The above experimental results show that the modified dyes are giving very good fluorescent signal discrimination to G-quadruplex DNA, which is not the same as their parent TO dye being nonselective for dsDNA and G-quadruplex DNA (Figures 1 and S6). In other words, the substituent on the TO molecule may either weaken the interaction with dsDNA/ssDNA or may result in the loss of fluorescence even if strong binding happens. To better understand how the structural changes lead to fluorescent discrimination on nucleic acid binding, molecular docking studies were performed to elucidate the interaction difference

between the dye and G-quadruplex DNA as well as duplex DNA. Previous studies reported that **TO** prefers to stack on the G-quartet,^{41,42} which is in accord with our docking results shown in Figure 6A,C.

As compared to **TO**, **4a** with a *p*-(dimethylamino)styryl substituent also stacks on the G-quartet in a very similar fashion, except that the styrene substitution contributes additionally to the stacking interaction with the G-quadruplex (Figure 6B,D) and its dimethylamine group is very close to the side of the G-quartet pocket. Previously, a NMR spectroscopy study suggested that a homodimeric thiazole orange dye (**TO**) acted as a duplex DNA intercalator with the **TO** chromophore stacking in the 5'-CpT-3' binding site⁴³ (Figure 7A). With

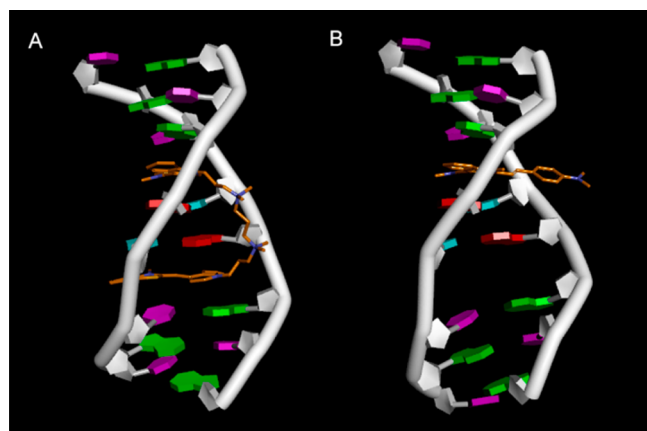


Figure 7. (A) A duplex DNA in complex with homodimeric thiazole orange dye (**TO**) from NMR spectroscopy studies, which shows that the **TO** chromophore is stacking in the 5'-CpT-3' binding site. (B) The same duplex DNA in complex with **4a** from molecular docking studies.

respect to our docking results, the **TO** molecule is almost completely embedded in the 5'-CpT-3' binding site of the dsDNA. Interestingly, **4a** also intercalates in the 5'-CpT-3' binding site in a very close orientation to **TO**; however, its substituent *p*-(dimethylamino)styryl at the ortho-position of **TO** completely projects out of the binding pocket without any interaction with duplex DNA (Figure 7B). The substituent is likely to interact with solvent molecules and thus leads to negative effects on both binding affinity and fluorescence signal due to its loosely bound manner as compared to the situation when bound with G-quadruplex (Figure 6B,C). The docking results indicate that the dye does have interactions with the dsDNA and also explains why the dyes induce a weak fluorescence signal in the study with dsDNA substrates. Similar results were also observed for **4b–4d**.

The comparison of the binding modes of the dyes on the G-quartet binding pocket of the telo21 G-quadruplex also gives meaningful information on how the substituents disturb the binding affinity. Figure 8 shows that the **TO** moiety is located in the center part of the G-quartet binding pocket, and the substituents with similar structure (*p*-(dimethylamino)styryl (**4a**), *p*-dimethylamino-phenyl-buta-1,3-dienyl (**4c**), and *p*-methylstyryl (**4d**)) are lying in almost the same manner. However, in **4b** the 2-vinyl-indole substituent is located in quite a different position, probably due to the bulky indole moiety. The amine group on the substituents appears to be beneficial for the interaction compared to 4-methylstyryl (**4d**). However, the performance of **4a** was found to be better than **4c**, because the substituent on **4c** is extended by two methylene units, resulting in the *p*-(dimethylamino)styryl moiety being located outside of the G-quartet binding pocket of telo21. In general, the binding modes found by the docking studies are able to explain the experimental observations on the intensity of the binding properties.

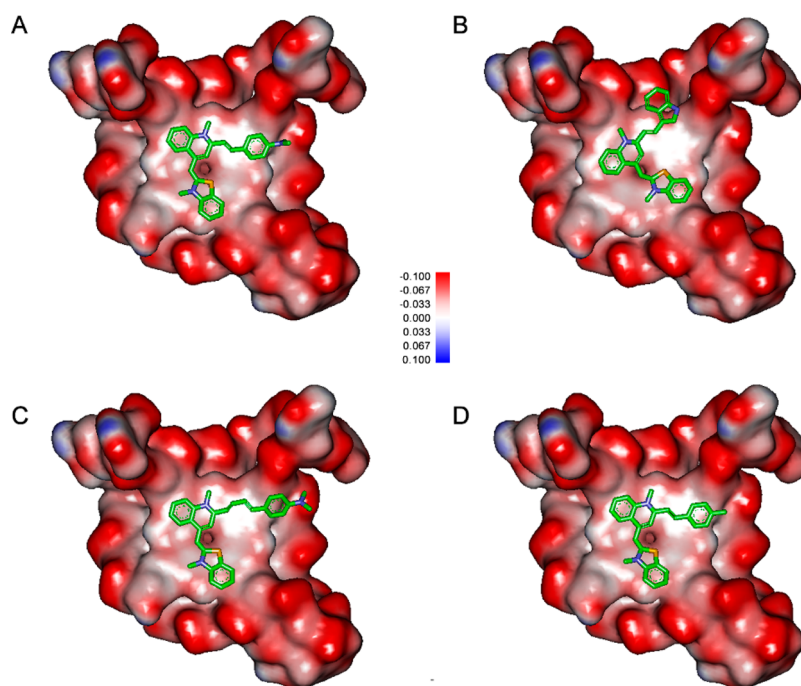


Figure 8. Comparison of binding modes of the dyes on the G-quartet binding pocket of telo21 G-quadruplex: (A) **4a**, (B) **4b**, (C) **4c**, and (D) **4d**. The interpolated charge of G-quadruplex was computed by DS viewer 3.5.

2.5. The Application of the Dye As a Fluorescent Staining Agent in Native Polyacrylamide Gel Electrophoresis (PAGE). The significant and selective fluorescence enhancement of the dyes when bound with quadruplex DNA structures led us to investigate the feasibility of using the dyes as fluorescent stains in native polyacrylamide gel electrophoresis (PAGE). Quadruplex DNA is poorly visualized in native gel electrophoresis by common fluorescent stains such as ethidium bromide, GelRed, or SYBR Safe. The experiments were performed using **4a**, since it has the best performance between the TO analogues. Figure 9 shows that poststaining of

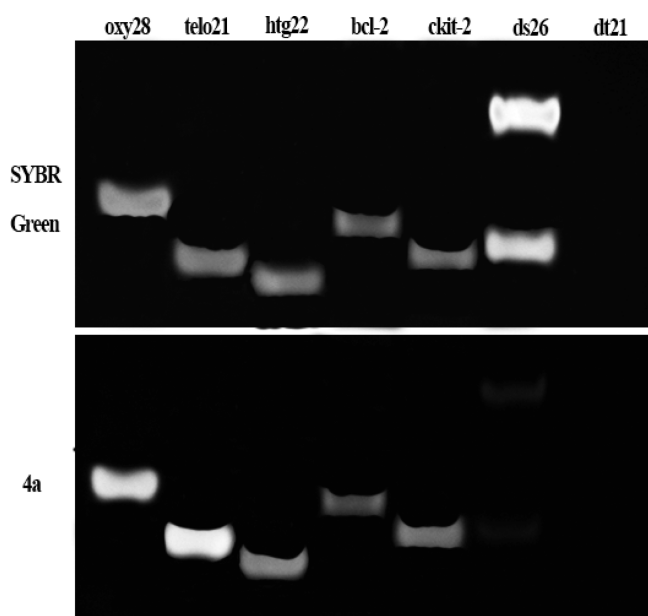


Figure 9. Gel electrophoresis (20% acrylamide in $1 \times$ TBE) of htg22, oxy28, telo21, bcl-2, ckit-2, dt21, and ds26 at a concentration $5.0 \mu\text{M}$ stained with SYBR green (top) and **4a** (bottom).

PAGE gels with a $5 \mu\text{M}$ solution of **4a** is able to selectively visualize the bands corresponding to G-quadruplexes including htg2, oxy28, telo21, bcl-2, and bcl-1. In contrast, almost no fluorescence was observed in the bands containing duplex-stranded DNA (ds26) and single-stranded DNA (dt21). The results highlight the potential of using **4a** as a G-quadruplex-selective fluorescent staining agent.

2.6. Application of the Dye in Live Cell Staining and Imaging. The application of the dye as a selective staining agent for the detection and imaging of G-quadruplexes in human prostate cancer cells PC3 was investigated. Fluorescence microscopy of the treated PC3 cells showed that both **4a** and DAPI are able to induce a strong fluorescence response in certain regions of the nucleus (Figure 10). The stained region corresponds to the nucleoli where rDNA undergoes transcription. It has been reported that guanine-rich rDNA may also adopt temporal quadruplex conformations.^{44,45} Moreover, from the costaining experiments with DAPI (a duplex DNA binder), a low fluorescence response was observed due to the nonspecific binding of the dye to duplex DNA. However, we cannot completely rule out the possibility that this weak signal is coming from the binding of **4a** with RNAs in the nucleus. For further clarification, experiments were performed whereby, after staining with **4a** and DAPI, the cells were subsequently treated with deoxyribonuclease (DNase) or ribonuclease (RNase). The enhanced fluorescence signals of **4a** in nucleoli clearly disappeared after DNase treatment, but not after RNase treatment (Figure 10). Therefore, this supports the premise that the dye enters the nucleus and interacts with the G-quadruplexes, resulting in the strong fluorescence signal. The results demonstrated that the new dyes have great potential for live cell staining and imaging, for the purpose of monitoring G-quadruplex DNA.

2.7. Investigation of Photostability. Photostability is an important factor when evaluating the usefulness of new fluorescent probes for live cell imaging. Since **4a** exhibited good cell tolerability (IC_{50} was about $0.598 \mu\text{M}$) at imaging

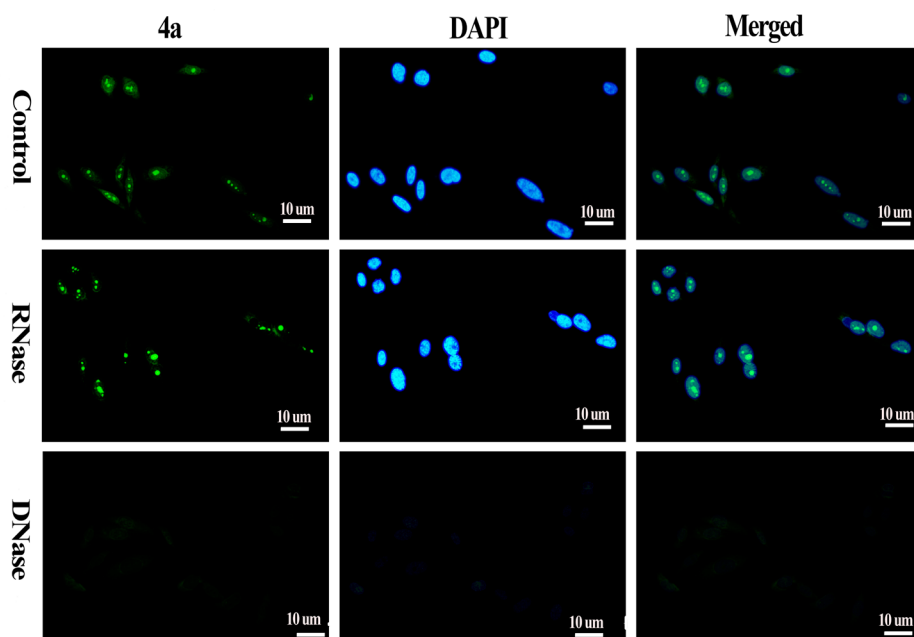


Figure 10. Fluorescence images of PC3 cells (fixed) stained with $5.0 \mu\text{M}$ of **4a** for 15 min and $1.0 \mu\text{g/mL}$ DAPI for 5 min without and with DNase or RNase treatment. $1000\times$ magnification was utilized in the imaging. Scale bar is $10 \mu\text{m}$.

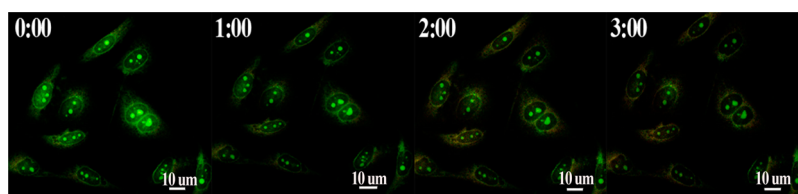


Figure 11. Photostability demonstration: The time-lapse imaging of nucleolus DNA in PC3 cells with **4a** in the range of 0–3 h. 1000× magnification was utilized in the imaging. Scale bar is 10 μm .

concentration after 24 h of incubation, we next examined the photostability of **4a** in cell imaging. Figure 11 shows the photostability of **4a** over 3 h when using PC3 cells. After 3 h, the fluorescence signal from **4a** in the nucleoli of PC cells was retained with sufficient intensity for clear visualization. The results demonstrated that **4a** is a robust dye for imaging of nucleoli G-quadruplex DNA in live cells and is particularly attractive for experiments requiring longer irradiation times.

Conclusions. In conclusion, a series of new fluorescent dyes were synthesized by introducing different styryl moieties at the ortho-position of thiazole orange. The compounds show very good fluorescence discrimination toward G-quadruplex DNA rather than dsDNA, exhibit high relative quantum yields upon binding with G-quadruplexes, and give excellent G-quadruplex stabilization as indicated by the larger ΔT_m values. A modeling study on the interaction of the dyes with DNA illustrates the influence of the introduced ancillary substituent at the ortho-position of thiazole orange on the binding discrimination between dsDNA and G-quadruplex DNA. In addition, the potential application of the dyes as *in vitro* biochemical reagents was successfully demonstrated by native PAGE experiments and live cell staining and imaging. The results indicate that these new dyes can be utilized for G-quadruplex specific biomolecular sensing and cell imaging.

METHODS FOR LIGAND SYNTHESIS

Synthesis of 4-Chloro-1,2-dimethylquinolin-1-ium Iodide

(1). To the solution of 4-chloro-2-methylquinoline (0.2 g, 1.12 mmol) in sulfolane (10 mL) was added iodomethane (0.42 mL, 6.74 mmol). The reaction mixture was stirred at 50 °C for 18 h and then cooled. Anhydrous ether was added to the reaction mixture and the solids collected by suction filtration, washed with anhydrous ether, and dried *in vacuo* to give compound **1** (0.36 g, 95.8%). mp = 245–247 °C. ^1H NMR (400 MHz, DMSO- d_6): δ 8.56 (d, J = 8.4 Hz, 1H), 8.46 (d, J = 8.3 Hz, 1H), 8.22 (t, J = 8.1 Hz, 1H), 8.01 (t, J = 7.9 Hz, 1H), 7.55 (s, J = 7.4 Hz, 1H), 4.20 (s, 3H), 2.68 (s, 3H). ESI-MS: m/z 192.1 $[\text{M} - \text{I}]^+$.

Synthesis of 1,2-Dimethylbenzothiazol-1-ium Iodide (2). A mixture of 2-methylbenzothiazole (0.25 g, 1.68 mmol), iodomethane (0.63 mL, 10.08 mmol), and anhydrous ethanol (10 mL) was stirred at reflux temperature for 15 h. After cooling, the mixture was dried over anhydrous ethanol and chloroform oscillating suction filtered. The precipitate was washed with chloroform and with a small amount of ethanol and vacuum-dried to give compound **2** (0.448 g, 91.7%). mp = 232–235 °C. ^1H NMR (400 MHz, DMSO- d_6): δ 8.44 (d, J = 8.1 Hz, 1H), 8.30 (d, J = 8.4 Hz, 1H), 7.90 (t, J = 7.8 Hz, 1H), 7.81 (t, J = 7.7 Hz, 1H), 4.20 (s, 3H), 3.17 (s, 3H). ESI-MS: m/z 164.4 $[\text{M} - \text{I}]^+$.

Synthesis of (Z)-1,2-Dimethyl-4-((3-methylbenzo[d]thiazol-2(3H)-ylidene)methyl)quinolin-1-ium Iodide (3). Compound **1** (0.5 g, 1.60 mmol), **2** (0.5 g, 1.72 mmol), and aqueous sodium bicarbonate solution (0.5 mol/L, 2 mL) were mixed with 10 mL of methanol. The mixture was stirred at RT for about 1 h. To the reaction solution, 4 mL of saturated KI solution was added. The mixture was then stirred for about 15 min. The solid obtained was collected by filtration, washed with water and acetone, and vacuum-dried to give compound **3** (0.49 g, 92.5%). mp = 268–270 °C. ^1H

NMR (400 MHz, DMSO- d_6): δ 8.77 (d, J = 8.3 Hz, 1H), 8.18 (d, J = 8.7 Hz, 1H), 8.02–7.96 (m, 2H), 7.74 (d, J = 8.2 Hz, 2H), 7.59 (t, J = 7.7 Hz, 1H), 7.39 (t, J = 7.5 Hz, 1H), 7.34 (s, 1H), 6.85 (s, 1H), 4.07 (s, 3H), 3.98 (s, 3H), 2.87 (s, 3H). ESI-MS: m/z 319.0 $[\text{M} - \text{I}]^+$.

General Procedures for Synthesis of Target Compounds 4a–4d. A mixture of **3** (0.072 g, 0.16 mmol), 4-methylpiperidine (0.5 mL), and *n*-butanol (10 mL) was stirred at RT. The chosen aldehyde (0.32 mmol) was added into the mixture and refluxed for 3 h. After the mixture was cooled and suction filtered, the solid was washed with *n*-butanol. The precipitate was purified by using column chromatography to afford the pure target compounds **4a–4d**.

Synthesis of N-Methyl-2-((E)-4-(dimethylamino)styryl)-4-((Z)-(3-methylbenzo[d]thiazol-2(3H)-ylidene)methyl)quinolin-1-ium Iodide (4a). Purple solid, yield 90%. mp = 301–304 °C. ^1H NMR (400 MHz, DMSO- d_6): δ 8.73 (d, J = 7.8 Hz, 1H), 8.14 (d, J = 8.4 Hz, 1H), 8.06–8.02 (m, 1H), 8.00–7.95 (m, 1H), 7.87 (d, J = 8.5 Hz, 2H), 7.76–7.68 (m, 3H), 7.64 (s, 1H), 7.61–7.55 (m, 2H), 7.42–7.35 (m, 3H), 6.87 (s, 1H), 4.13 (s, 3H), 3.97 (d, J = 3.7 Hz, 3H), 2.56 (s, 6H). ^{13}C NMR (100 MHz, DMSO- d_6): δ 158.77, 153.24, 152.30, 147.53, 142.83, 141.10, 139.57, 133.43, 130.97, 128.40, 126.63, 125.57, 124.30, 124.08, 123.92, 123.38, 123.09, 118.93, 115.07, 112.69, 112.16, 108.03, 87.58, 38.28, 33.91. HRMS (ESI) m/z calcd for $\text{C}_{29}\text{H}_{28}\text{N}_3\text{S}^+$ ($[\text{M} - \text{I}]^+$): 450.1998. Found: 450.1986. HPLC retention time of **4a** was 5.439 min.

Synthesis of 2-((E)-2-(1H-Indol-3-yl)vinyl)-1-methyl-4-((Z)-(3-methylbenzo[d]thiazol-2(3H)-ylidene)methyl)quinolin-1-ium Iodide (4b). Purple solid, yield 85%. mp = 298–302 °C. ^1H NMR (400 MHz, DMSO- d_6): δ 11.97 (s, 1H), 8.62 (d, J = 8.4 Hz, 1H), 8.20 (s, 1H), 8.09 (d, J = 7.3 Hz, 1H), 8.03 (d, J = 8.8 Hz, 1H), 7.98 (d, J = 7.8 Hz, 1H), 7.88 (dd, J = 15.5, 5.5 Hz, 2H), 7.63 (t, J = 7.6 Hz, 1H), 7.51 (q, J = 8.4 Hz, 4H), 7.33–7.23 (m, 4H), 6.70 (d, J = 8.5 Hz, 1H), 4.07 (s, 3H), 3.83 (s, 3H). ^{13}C NMR (100 MHz, DMSO- d_6): δ 158.38, 153.65, 147.23, 140.96, 139.40, 136.84, 133.30, 128.29, 126.47, 125.49, 125.13, 124.14, 123.92, 123.80, 123.38, 123.26, 121.71, 120.70, 118.78, 114.21, 113.98, 113.05, 112.54, 107.63, 87.39, 38.20, 33.84. HRMS (ESI) m/z calcd for $\text{C}_{29}\text{H}_{24}\text{N}_3\text{S}^+$ ($[\text{M} - \text{I}]^+$): 446.1685. Found: 446.1674. HPLC retention time of **4b** was 3.608 min.

Synthesis of 2-((1E,3E)-4-(4-(Dimethylamino)phenyl)buta-1,3-dien-1-yl)-1-methyl-4-((Z)-(3-methylbenzo[d]thiazol-2(3H)-ylidene)methyl)quinolin-1-ium Iodide (4c). Purple solid, yield 88%. mp = 289–293 °C. ^1H NMR (400 MHz, DMSO- d_6): δ 8.70 (d, J = 8.5 Hz, 1H), 8.12 (d, J = 8.9 Hz, 1H), 8.07 (d, J = 7.9 Hz, 1H), 7.95 (t, J = 7.8 Hz, 1H), 7.73–7.68 (m, 2H), 7.59 (dd, J = 13.5, 7.0 Hz, 3H), 7.49 (d, J = 8.7 Hz, 2H), 7.39 (t, J = 7.6 Hz, 1H), 7.17 (dd, J = 24.7, 13.8 Hz, 3H), 6.83–6.76 (m, 3H), 4.09 (d, J = 8.5 Hz, 3H), 3.96 (s, 3H), 3.00 (d, J = 11.7 Hz, 6H). ^{13}C NMR (100 MHz, DMSO- d_6): δ 158.75, 152.13, 151.49, 147.13, 143.68, 142.22, 140.98, 139.42, 133.35, 129.38, 128.39, 126.59, 125.49, 124.30, 124.08, 124.00, 123.81, 123.62, 123.41, 120.93, 118.77, 112.78, 112.53, 107.66, 87.68, 37.99, 33.94. HRMS (ESI) m/z calcd for $\text{C}_{31}\text{H}_{30}\text{N}_3\text{S}^+$ ($[\text{M} - \text{I}]^+$): 476.2154. Found: 476.2144. HPLC retention time of **4c** was 4.889 min.

Synthesis of 1-Methyl-4-((Z)-(3-methylbenzo[d]thiazol-2(3H)-ylidene)methyl)-2-((E)-4-methylstyryl)quinolin-1-ium Iodide (4d). Purple solid, yield 83%. mp = 273–276 °C. ^1H NMR (400 MHz, DMSO- d_6): δ 8.77 (d, J = 8.3 Hz, 1H), 8.19 (d, J = 8.8 Hz, 1H), 8.07 (d, J = 7.8 Hz, 1H), 8.00 (t, J = 7.9 Hz, 1H), 7.85 (d, J = 7.9 Hz, 2H), 7.75 (dd, J = 8.7, 5.6 Hz, 3H), 7.63 (dt, J = 15.6, 9.9 Hz, 3H), 7.43–7.34 (m, 3H), 6.92 (s, 1H), 4.17 (s, 3H), 4.00 (d, J = 8.1 Hz, 3H), 2.41 (s, 3H). ^{13}C NMR (100 MHz, DMSO- d_6): δ 159.88, 152.60, 148.26,

141.32, 141.05, 140.79, 139.52, 133.74, 132.99, 130.03, 128.95, 128.55, 126.97, 125.69, 124.69, 124.27, 124.01, 123.48, 121.10, 119.03, 113.14, 108.44, 88.27, 38.53, 34.12, 21.57. HRMS (ESI) m/z calcd for $C_{28}H_{25}N_5S^+$ ($[M - 1]^+$): 421.1732. Found: 421.1721. HPLC retention time of **4d** was 3.384 min.

Modeling Method. The crystal structure of telo21 G-quadruplex DNA 5'-d[GGG(TTAGGG)3]-3' (PDB id 4DA3)⁴⁶ in complex with naphthalene diimide ligands was used as the G-quadruplex target. The NMR structure of duplex DNA 5'-d(CGCTAGCG)-3' in complex with homodimeric thiazole orange dye (TO) (PDB id: 108D) was used for the modeling of intercalation interaction. Docking studies were performed using the AUTODOCK 4.0 program.⁴⁷ The dimensions of the active site box were chosen to be large enough to encompass the entire G-quadruplex DNA and the active site of duplex DNA. All docking calculations were carried out using the Lamarckian genetic algorithm (LGA). A maximum number of 2 500 000 energy evaluation was used. Each docking experiment includes 200 independent runs.

■ ASSOCIATED CONTENT

● Supporting Information

The Supporting Information is available free of charge on the ACS Publications website at DOI: 10.1021/acscchembio.5b00987.

Additional experimental details, Figures S1–S10, and Tables S1–S3 (PDF)

■ AUTHOR INFORMATION

Corresponding Authors

*Tel.: +86-20-39322235. E-mail: luyj@gdut.edu.cn.

*Tel.: +852-2948-8401. Fax: +852-2948-7676. E-mail: wingleung@ied.edu.hk.

Notes

The authors declare no competing financial interest.

■ ACKNOWLEDGMENTS

We acknowledge the support received from the National Nature Science Foundation of China (21102021 and 81473082), Nature Science Foundation of Guangdong Province, China (S2012010010200), and Science and Technology Program of Guangdong Province (2012B020306007). The authors are also grateful to the support from Guangdong Province Higher Education “Qianbaishi Engineering” project, and Guangdong University of Technology “Pei Ying Yu Cai” Project. We thank the Shared Hierarchical Academic Research Computing Network (SHARCNET, www.sharcnet.ca) for allocation of computer resources. J.-Q.H. thanks Prostate Cancer Canada for fellowship support.

■ REFERENCES

- (1) Cao, Y. C., Jin, R., and Mirkin, C. A. (2002) Nanoparticles with Raman spectroscopic fingerprints for DNA and RNA detection. *Science* 297, 1536–1540.
- (2) Liu, S., Zhang, C., Ming, J., Wang, C., Liu, T., and Li, F. (2013) Amplified detection of DNA by an analyte-induced Y-shaped junction probe assembly followed with a nicking endonuclease-mediated autocatalytic recycling process. *Chem. Commun.* 49, 7947–7949.
- (3) Hou, T., Wang, X., Liu, X., Liu, S., Du, Z., and Li, F. (2013) A label-free and colorimetric turn-on assay for coralyne based on coralyne-induced formation of peroxidase-mimicking split DNAzyme. *Analyst* 138, 4728–4731.
- (4) Wang, X., Hou, T., Lu, T., and Li, F. (2014) Autonomous exonuclease III-assisted isothermal cycling signal amplification: a facile and highly sensitive fluorescence DNA glycosylase activity assay. *Anal. Chem.* 86, 9626–9631.
- (5) Parkinson, G. N., Lee, M. P., and Neidle, S. (2002) Crystal structure of parallel quadruplexes from human telomeric DNA. *Nature* 417, 876–880.
- (6) Burge, S., Parkinson, G. N., Hazel, P., Todd, A. K., and Neidle, S. (2006) Quadruplex DNA: sequence, topology and structure. *Nucleic Acids Res.* 34, 5402–5415.
- (7) Brooks, T. A., Kendrick, S., and Hurley, L. (2010) Making sense of G-quadruplex and i-motif functions in oncogene promoters. *FEBS J.* 277, 3459–3469.
- (8) Huppert, J. L., and Balasubramanian, S. (2007) G-quadruplexes in promoters throughout the human genome. *Nucleic Acids Res.* 35, 406–413.
- (9) Eddy, J., and Maizels, N. (2008) Conserved elements with potential to form polymorphic G-quadruplex structures in the first intron of human genes. *Nucleic Acids Res.* 36, 1321–1333.
- (10) Huppert, J. L., Bugaut, A., Kumari, S., and Balasubramanian, S. (2008) G-quadruplexes: the beginning and end of UTRs. *Nucleic Acids Res.* 36, 6260–6268.
- (11) Riou, J. F. (2004) G-quadruplex interacting agents targeting the telomeric G-overhang are more than simple telomerase inhibitors. *Curr. Med. Chem.: Anti-Cancer Agents* 4, 439–443.
- (12) Dunnick, W., Hertz, G. Z., Scappino, L., and Gritzmacher, C. (1993) DNA sequences at immunoglobulin switch region recombination sites. *Nucleic Acids Res.* 21, 365–372.
- (13) Rawal, P., Kummarasetti, V. B. R., Ravindran, J., Kumar, N., Halder, K., Sharma, R., Mukerji, M., Das, S. K., and Chowdhury, S. (2006) Genome-wide prediction of G4 DNA as regulatory motifs: role in Escherichia coli global regulation. *Genome Res.* 16, 644–655.
- (14) Hanakahi, L. A., Sun, H., and Maizels, N. (1999) High affinity interactions of nucleolin with GG-paired rDNA. *J. Biol. Chem.* 274, 15908–15912.
- (15) Rezler, E. M., Bearss, D. J., and Hurley, L. H. (2002) Telomeres and telomerases as drug targets. *Curr. Opin. Pharmacol.* 2, 415–423.
- (16) Cairns, D., Anderson, R. J., Perry, P. J., and Jenkins, T. C. (2002) Molecular modelling and cytotoxicity of substituted anthraquinones as inhibitors of human telomerase. *Curr. Pharm. Des.* 8, 2491–2504.
- (17) Rezler, E. M., Seenisamy, J., Bashyam, S., Kim, M. Y., White, E., Wilson, W. D., and Hurley, L. H. (2005) Telomestatin and diseleno saphyrin bind selectively to two different forms of the human telomeric G-quadruplex structure. *J. Am. Chem. Soc.* 127, 9439–9447.
- (18) Ou, T. M., Lu, Y. J., Tan, J. H., Huang, Z. S., Wong, K. Y., and Gu, L. Q. (2008) G-quadruplexes: Targets in anticancer drug design. *ChemMedChem* 3, 690–713.
- (19) Fu, R., Li, T., and Park, H. G. (2009) An ultrasensitive DNAzyme-based colorimetric strategy for nucleic acid detection. *Chem. Commun.* 39, 5838–5840.
- (20) Lu, Y. J., Hu, D. P., Deng, Q., Wang, Z. Y., Huang, B. H., Fang, Y. X., Zhang, K., and Wong, W.-L. (2015) Sensitive and selective detection of uracil-DNA glycosylase activity with a new pyridinium luminescent switch-on molecular probe. *Analyst* 140, 5998–6004.
- (21) Yan, J. W., Chen, S. B., Liu, H. Y., Ye, W. J., Ou, T. M., Tan, J. H., Li, D., Gu, L. Q., and Huang, Z. S. (2014) Development of a new colorimetric and red-emitting fluorescent dual probe for G-quadruplex nucleic acids. *Chem. Commun.* 50, 6927–6930.
- (22) Guo, J.-H., Zhu, L.-N., Kong, D.-M., and Shen, H.-Y. (2009) Triphenylmethane dyes as fluorescent probes for G-quadruplex recognition. *Talanta* 80, 607–613.
- (23) Lai, H., Xiao, Y. J., Yan, S. Y., Tian, F. F., Zhong, C., Liu, Y., Weng, X., and Zhou, X. (2014) Symmetric cyanovinyl-pyridinium triphenylamine: a novel fluorescent switch-on probe for an antiparallel G-quadruplex. *Analyst* 139, 1834–1838.
- (24) Chen, S. B., Wu, W. B., Hu, M. H., Ou, T. M., Gu, L. Q., Tan, J. H., and Huang, Z. S. (2014) Discovery of a new fluorescent light-up probe specific to parallel G-quadruplexes. *Chem. Commun.* 50, 12173–12176.
- (25) Lee, L. G., Chen, C.-H., and Chiu, L. A. (1986) Thiazole orange: a new dye for reticulocyte analysis. *Cytometry* 7, 508–517.

- (26) Nygren, J., Svanvik, N., and Kubista, M. (1998) The interactions between the fluorescent dye thiazole orange and DNA. *Biopolymers* 46, 39–51.
- (27) Kohler, O., Jarikote, D. V., and Seitz, O. (2005) Forced intercalation probes (FIT probes): thiazole orange as a fluorescent base in peptide nucleic acids for homogeneous single-nucleotide-polymorphism detection. *ChemBioChem* 6, 69–77.
- (28) Lu, Y. J., Wang, Z. Y., Hu, D. P., Deng, Q., Huang, B. H., Fang, Y. X., Zhang, K., Wong, W.-L., and Chow, C.-F. (2015) Benzothiazole-substituted benzofuroquinolinium dyes as new fluorescent probes for G-quadruplex DNA. *Dyes Pigm.* 122, 94–102.
- (29) Lu, Y. J., Yan, S. C., Chan, F. Y., Zou, L., Chung, W. H., Wong, W.-L., Qiu, B., Sun, N., Chan, P.-H., Huang, Z. S., Gu, L. Q., and Wong, K.-Y. (2011) Benzothiazole-substituted benzofuroquinolinium dye: a selective switch-on fluorescent probe for G-quadruplex. *Chem. Commun.* 47, 4971–4973.
- (30) Yan, J. W., Ye, W. J., Chen, S. B., et al. (2012) Development of a universal colorimetric indicator for G-quadruplex structures by the fusion of thiazole orange and isaindigotone skeleton. *Anal. Chem.* 84, 6288–6292.
- (31) Unger-angel, L., Rout, B., Ilani, T., Eisenstein, M., Motiei, L., and Margulies, D. (2015) Protein recognition by bivalent, turn-on fluorescent molecular probes. *Chem. Sci.* 6, 5419–5425.
- (32) Laguerre, A., Stefan, L., Larrouy, M., Genest, D., Novotna, J., Pirrotta, M., and Monchaud, D. (2014) A twice-as-smart synthetic G-quartet: pyroTASQ is both a smart quadruplex ligand and a smart fluorescent probe. *J. Am. Chem. Soc.* 136, 12406–12414.
- (33) Yang, P., De Cian, A., Teulade-Fichou, M. P., Mergny, J. L., and Monchaud, D. (2009) Engineering bisquinolinium/thiazole orange conjugates for fluorescent sensing of G-quadruplex DNA. *Angew. Chem., Int. Ed.* 48, 2188–2193.
- (34) Lu, Y. J., Deng, Q., Hu, D. P., Wang, Z. Y., Huang, B. H., Du, Zh.Y., Fang, Y. X., Wong, W.-L., Zhang, K., and Chow, C.-F. (2015) A molecular fluorescent dye for specific staining and imaging of RNA in live cells: a novel ligand integration from classical thiazole orange and styryl compounds. *Chem. Commun.* 51, 15241–15244.
- (35) Lee, J. W., Jung, M., Rosania, G. R., and Chang, Y.-T. (2003) Development of novel cell-permeable DNA selective dyes using combinatorial synthesis and cell based screening. *Chem. Commun.* 15, 1852–1853.
- (36) Zhang, W. J., Ou, T. M., Lu, Y. J., Huang, Y. Y., Wu, W. B., Huang, Z. S., Zhou, J. L., Wong, K. Y., and Gu, L. Q. (2007) 9-substituted berberine derivatives as G-quadruplex stabilizing ligands in telomeric DNA. *Bioorg. Med. Chem.* 15, 5493–5501.
- (37) Teulade-Fichou, M. P., Carrasco, C., Guittat, L., Bailly, C., Alberti, P., Mergny, J. L., David, A., Lehn, J. M., and Wilson, W. D. (2003) Selective recognition of G-quadruplex telomeric DNA by a bis(quinacridine) macrocycle. *J. Am. Chem. Soc.* 125, 4732–4740.
- (38) Koepfel, K., Riou, J. F., Laoui, A., Mailliet, P., Arimondo, P. B., Labit, D., Petitgenet, O., Hélène, C., and Mergny, J. L. (2001) Ethidium derivatives bind to G-quartets, inhibit telomerase and act as fluorescent probes for quadruplexes. *Nucleic Acids Res.* 29, 1087–1096.
- (39) Mergny, J. L., Lacroix, L., Teulade-Fichou, M. P., Hounsou, C., Guittat, L., Hoarau, M., Arimondo, P. B., Vigneron, J. P., Lehn, J. M., Riou, J. F., Garestier, T., and Hélène, C. (2001) Telomerase inhibitors based on quadruplex ligands selected by a fluorescence assay. *Proc. Natl. Acad. Sci. U. S. A.* 98, 3062–3067.
- (40) Balagurumoorthy, P., Brahmachari, S. K., Mohanty, D., Bansal, M., and Sasisekharan, V. (1992) Hairpin and parallel quartet structures for telomeric sequences. *Nucleic Acids Res.* 20, 4061–4067.
- (41) Nasiri, H. R., Bell, N. M., McLuckie, K. I., Husby, J., Abell, C., Neidle, S., and Balasubramanian, S. (2014) Targeting a c-MYC G-quadruplex DNA with a fragment library. *Chem. Commun.* 50, 1704–1709.
- (42) Monchaud, D., Allain, C., and Teulade-Fichou, M. P. (2006) Development of a fluorescent intercalator displacement assay (G4-FID) for establishing quadruplex-DNA affinity and selectivity of putative ligands. *Bioorg. Med. Chem. Lett.* 16, 4842–4845.
- (43) Spielmann, H. P., Wemmer, D. E., and Jacobsen, J. P. (1995) Solution structure of a DNA complex with the fluorescent bis-intercalator TOTO determined by NMR spectroscopy. *Biochemistry* 34, 8542–8553.
- (44) Drygin, D., Siddiqui-Jain, A., O'Brien, S., Schwaebe, M., Lin, A., Bliesath, J., Ho, C. B., Proffitt, C., Trent, K., Whitten, J. P., Lim, J. K. C., Von Hoff, D., Anderes, K., and Rice, W. G. (2009) Anticancer activity of CX-3543: a direct inhibitor of rRNA biogenesis. *Cancer Res.* 69, 7653–7661.
- (45) Hanakahi, L. A., Sun, H., and Maizels, N. (1999) High affinity interactions of nucleolin with GG-paired rDNA. *J. Biol. Chem.* 274, 15908–15912.
- (46) Micco, M., Collie, W. G., Dale, A. G., Ohnmacht, S. A., Pazitna, I., Gunaratnam, M., Reszka, A. P., and Neidle, S. (2013) Structure-based design and evaluation of naphthalene diimide G-quadruplex ligands as telomere targeting agents in pancreatic cancer cells. *J. Med. Chem.* 56, 2959–2974.
- (47) Olsen, C. M., and Marky, L. A. (2010) Monitoring the temperature unfolding of G-quadruplexes by UV and circular dichroism spectroscopies and calorimetry techniques. *Methods Mol. Biol.* 608, 147–158.